A&A 395, 117–127 (2002)
DOI: 10.1051/0004-6361:20021295

Astronomy & Astrophysics

Orbital motion in symbiotic Mira systems⋆

H. M. Schmid and H. Schild

Institut für Astronomie, ETH-Zentrum, 8092 Zürich, Switzerland

Received 28 June 2002 / Accepted 1 August 2002

Abstract. We present new spectropolarimetry of the Raman lines for seven symbiotic Miras, combine it with earlier data and review the polarimetric changes. All systems show slow and usually steady angular variations which are most easily interpreted as a reflection of the orbital motion. We measure angular rotation rates of typically 1 to 5°/yr. Small position angle changes are seen in Hen2-106 and RR Tel, while Hen2-38 and Hen2-127 have high rotation rates. Although our database spreads over a time span of almost 10 years, we still cover only a fraction of a typical D-type orbit. Since we expect elliptical orbits, it is too early to extrapolate to an orbital period for any individual object. In a statistical sense, however, our mean angular rotation rate shows that an average orbital period for a symbiotic Mira is 150 years. We also determine the position angle of the binary axes as projected onto the sky. Our polarimetry finally suggests that the binary axes of the systems V1016 Cyg and Hen2-38 are not far from parallel to the line of sight (conjunction), whereas the binary axes of RR Tel and AS 210 lie approximately at an angle of 90° to the line of sight.

Key words. stars: binaries: symbiotic – stars: AGB and post-AGB – stars: circumstellar matter – polarization – scattering

1. Introduction

Long period binaries consisting of an active white dwarf and a red giant are called symbiotic systems. In a subgroup of these systems the red giant is a Mira variable (Whitelock 1987). The symbiotic Miras, also known as D-type symbiotic systems, show strong dust emission. The mere size of the Mira variable requires that the binary separation is large in order to avoid merging of the two components within a short time scale. However, the separation must also have an upper limit beyond which mass transfer and accretion is insufficient and nova-like activity of the white dwarf becomes impossible. Another manifestation of binary interaction is the presence of complicated circumstellar structures (e.g. Corradi et al. 1999, 2001; Eyres et al. 2001).

Despite a lot of investigational efforts dedicated to symbiotic Miras, their orbital periods, the binary separation, and the orientation of the stellar components remain very poorly known. Orbital periods can normally be determined via radial velocity measurements, but in the case of symbiotic Miras, the small orbital velocities are completely overwhelmed by atmospheric pulsations and turbulence. Knowledge of the binary parameters is however highly desirable and indispensable for a quantitative interpretation of the observed activity and the geometric distribution of the circumstellar material.

In this paper we examine spectropolarimetric observations of the Raman scattered O VI emission lines $\lambda\lambda$6825, 7082. The long-term behaviour of the polarization of these lines reflects the binary motion and constrains the system orientation. The two lines are produced by a Raman scattering process of the O VI $\lambda\lambda$1032, 1038 resonance lines by neutral hydrogen (Schmid 1989). Raman scattering is a dipole type scattering process and therefore produces for right angle scattering ($\alpha = 90°$) a light polarization of 100% with a polarization angle perpendicular to the scattering plane. Forward and backward scatterings ($\alpha = 0°$ or 180°) are unpolarized, while the polarization is intermediate at intermediate angles. The basic link between polarization and binary configuration is therefore quite simple, if the O VI emission is associated with the hot component and the scattering H^0-atoms with the red giant. The polarization structure of the Raman lines was simulated for various system geometries with more complicated models that included Doppler shifts introduced by particle motions, multiple scattering effects, and geometric compensation due to polarization from unresolved scattering regions (Schmid 1995, 1996; Harries & Howarth 1997; Lee & Lee 1997a,b). These models strongly confirm the basic scattering geometry outlined above, where the far-UV O VI line radiation is produced in the ionized region near the active white dwarf and converted into the two red Raman lines by neutral hydrogen in the extended atmosphere and wind of the red giant.

According to this basic model the polarization angle in the Raman line defines the orientation of the scattering geometry

Send offprint requests to: H. M. Schmid,
e-mail: schmid@astro.phys.ethz.ch

⋆ Based on observations obtained at the ESO 3.6 m Telescope at La Silla, Chile (ESO program 63.H-0034), the 3.9 m Anglo-Australian Telescope at Siding Spring, Australia, and the 4.2 m William Herschel Telescope at La Palma, Canary Islands.

Table 1. Log of the spectropolarimetric Raman line observations of D-type symbiotics. The entries are described in the text. The last column and the footnotes give references to previous papers describing the data of the objects in the corresponding line. Alternative target names: Hen2-38 = V366 Car, Hen2-106 = V835 Cen.

date	telescope	instrument	res. [Å]	objects	ref.
18.8.1991	WHT	ISIS	4.5	V1016 Cyg	SS94
28.6–1.7.1992	ESO 3.6 m	EFOSC1	7.4	Hen2-38, Hen2-106, Hen2-127, RR Tel	SS94
17.9/5.10.1992	WHT	ISIS	0.65	V1016 Cyg	SS96
27.5.1993	WHT	ISIS	0.65	AS 210,	
				V1016 Cyg	SS96
22.8.1993	WHT	ISIS	0.65	AS 210	
18.9.1994	WHT	ISIS	0.65	V1016 Cyg	SS96
15.1.1995	AAT	RGO	1.7	Hen2-38, Hen2-106	
8.3.1995	AAT	RGO	1.7	Hen2-106, Hen2-127, AS 210,	
				RR Tel	E&95
25/26.6.1997	WHT	ISIS	0.65	AS 210, V1016 Cyg	
30.6.1998	WHT	ISIS	1.6	AS 210, V1016 Cyg	
				HM Sge	S&00
17.6.1999	ESO 3.6 m	EFOSC2	5.5	He-38, Hen2-106, Hen2-127, AS 210, RR Tel, HM Sge	
21/22.8.1999	VLT1	FORS1	4.5	RR Tel	

SS94: Schmid & Schild (1994); SS96: Schild & Schmid (1996); E&95: Espey et al. (1995); S&00: Schmid et al. (2000).

which is closely linked to the relative position of the two binary components. Phase locked variations can be used to determine the orbital motion. In spite of the long periods of symbiotic Miras, first estimates of the period can already be made after a relatively small rotation of the polarization angle. We combine here new spectropolarimetry with already published earlier data and focus on the regular long term effects.

2. Observations

The spectropolarimetric data for the symbiotics discussed here were obtained during the last decade with Cassegrain instruments at four different telescopes. At the 4.2 m William Herschel Telescope (WHT) and the 3.9 m Anglo-Australian Telescope (AAT) we used the ISIS and RGO grating spectrographs respectively, equipped with a special aperture plate, a rotatable half-wave plate and a calcite block for spectropolarimetry. At ESO, the data were obtained with the multi-mode focal reducer imager and grism spectrographs EFOSC1 and EFOSC2 at the 3.6 m Telescope and FORS1 at the 8.2 m "Antu" Very Large Telescope Unit 1 (VLT1). EFOSC2 and FORS1 were used with a special slit aperture (EFOSC) or movable slitlets (FORS1), a rotatable half-wave plate and a Wollaston prism. EFOSC1 had no rotatable half-wave plate, so that the polarization at different angles was obtained by rotating the entire Cassegrain instrument (see Schmid & Schild 1994).

The observational details are summarised in Table 1. The spectral resolution is determined from the line widths of an arc-lamp spectrum taken with the same slit as the targets. The resolution is significantly higher for the grating spectrographs, except for the WHT observations from August 1991 which suffered from a focusing error. Further observational details can be found in the references to previously published spectropolarimetry (see Table 1).

One spectropolarimetric measurement consists of a set of four observations taken at half-wave plate angles of 0°, 45°, 22.5° and 67.5° (except for the EFOSC1 observations). The subsequent calcite block or Wollaston prism generates two beams with perpendicular polarization. Exposures with the half-wave plate at 0°, 45° yield Stokes Q and the other two yield Stokes U.

The data from the ESO 3.6 m telescope, from the AAT, and from the WHT 1998 run were taken within observing programs, where full nights were allocated to spectropolarimetry of symbiotic stars and related objects. The RR Tel data from the VLT1 were taken as a short calibration observation for checking the zero angle of the instrument polarization within a spectropolarimetric program dedicated to AGN (Schmid et al. 2001). For all these observations we have taken a number of polarization standard stars in order to calibrate and correct accurately for the instrumental polarization. The remaining data were collected at the WHT during short runs of a few hours in service mode in the framework of a long term monitoring program. For these observations at least one polarized and one zero-polarization standard star were observed with the same instrumental set up.

The intrinsic instrument polarization was found to be of the order 0.1% or less in all cases. We estimate that the remaining systematic measuring error in the percentage polarization p is of this order. Only for the data of the EFOSC1 run from 1992, which were not taken with a rotatable half-wave plate, a higher uncertainty of about 0.35% must be expected. Due to the inferior measuring procedure the accuracy of these measurements is limited by residual fringing.

From observations of polarized standard stars we estimate that the residual systematic error in the polarization angle is only about $\Delta\theta \sim 1°$. This may seem rather optimistic since different lists of polarized standard stars sometimes disagree by up to a few degrees. However, we relied always on the same

Table 2. Mean continuum polarization in the spectral range 6600–7200 Å.

star	date	p_c [%]	θ_c [°]	ref.
Hen2-38	6/92	2.08	65.4	SS94*
	5/94	2.09	68.6	HH96
	1/95	2.25	68.1	
	6/99	2.11	68.1	
Hen2-106	6/92	2.45	62.6	SS94*
	5/94	2.81	65.6	HH96
	1/95	3.12	68.0	
	3/95	3.03	66.8	
	6/99	2.84	64.1	
Hen2-127	6/92	3.26	71.9	SS94*
	5/94	3.04	73.2	HH96
	3/95	3.16	71.9	
	6/99	2.68	76.3	
AS 210	5/93	1.61	53.0	
	8/93	1.20	39.4	
	5/94	1.04	52.7	HH96
	3/95	2.09	47.9	
	6/97	1.07	41.9	
	6/98	0.87	51.3	
	6/99	0.95	53.3	
HM Sge	7/93	1.17	48.3	
	7/95	1.13	43.9	
	6/98	1.03	47.5	
	6/99	1.00	41.0	
V1016 Cyg	8/91	0.29	100.5	SS94
	91-94	0.26	109	SS96
	6/97	0.69	84.5	
	6/98	0.37	106.4	
RR Tel	6/92	0.24	103	SS94
	5/94	0.23	127.5	HH96
	3/95	0.52	170.4	
	6/99	0.38	168.4	
	8/99	0.37	169.8	

∗: Not included for the evaluation of the interstellar polarization; SS94: Schmid & Schild (1994); HH96: Harries & Howarth (1996b); SS96: Schild & Schmid (1996).

standard stars and mainly those given in Hsu & Breger (1982). Thus, at least for relative position angle changes the $\Delta\theta = 1°$ measuring error should be appropriate.

For objects with weak polarization signals the dominant error source is not systematic but due to the limited photon statistics. Other error sources that are not directly linked to the observational process arise in the definition of spectral features above a highly structured continuum, or in uncertainties in the interstellar polarization (see below).

3. Interstellar versus intrinsic polarization

Our data typically show a strong polarization signal in the Raman lines and a weak continuum polarization (see Fig. 1). If the continuum polarization is interstellar in origin, the Raman line polarization has to be corrected for it; if it is intrinsic to the object, no correction is necessary. Of course, the continuum polarization could be composed of a mixture of interstellar as well as intrinsic polarization and, unfortunately, there is no a priori way to separate the two. In the case of pure interstellar polarization, however, a number of conditions have to be fulfilled:

- the polarization does not vary with time;
- the spectral dependence of the relative polarization is smooth;
- the spectral dependence can be well described by the Serkowski law (Serkowski et al. 1975) and the position angle θ does not rotate with wavelength;
- surrounding stars with similar distances show a similar interstellar polarization pattern.

Some galactic regions have a complicated structure in the interstellar magnetic fields, so that the latter two conditions cannot be used without restriction. Occasionally, deviations of $p(\lambda)$ from a Serkowski law or a smooth rotation of the polarization angle with wavelength and/or a range in position angles for surrounding stars can be the result of the superposition of different interstellar components.

With our data we can in particular investigate whether we see temporal changes or spectral features in the continuum polarization attributable to an intrinsic component. We have measured the flux weighted mean continuum polarization for the range 6600–7200 Å in order to investigate the presence of time variability. Table 2 lists the corresponding polarization values together with the continuum polarization published in Harries & Howarth (1996b) for practically the same spectral range. Here, we do not use photo-polarimetric observations because the spectral windows are too different.

Hen2-38, Hen2-106 and Hen2-127 show no significant or at most very little $\Delta p \lesssim 0.3\%$, $\Delta\theta \lesssim 5°$ temporal variations in the continuum polarization. We also do not see any polarization features in the continuum. This suggests strongly that the continuum polarization is interstellar in origin. In the case of Hen2-106 and Hen2-127 this is supported by the interstellar polarization maps of surrounding stars (Schmid & Schild 1994; Harries & Howarth 1996b). For Hen2-38, the polarization maps show a different interstellar polarization pattern (see Harries & Howarth 1996b) but the surrounding stars are less distant than Hen2-38 and therefore not representative of the interstellar polarization. We therefore assume that for all three objects, Hen2-38, Hen2-106 and Hen2-127, the continuum polarization is entirely due to interstellar polarization. The adopted values given in Table 3 are the vector-means of the high-quality measurements (excluding the EFOSC1-data of SS94) given in Table 2.

For HM Sge the continuum polarization in the 6600–7200 Å range is practically constant with time, but at longer wavelengths spectropolarimetric features due to the red giant are visible. In Schmid et al. (2000) the continuum polarization is separated into an interstellar and an intrinsic component. We adopt here the interstellar polarization component $p_{is} = 1.0\%$ and $\theta_{is} = 42°$ from that work.

AS 210 displays large temporal continuum polarization changes of $\Delta p_c \approx 1\%$ (see Fig. 1). These variations are

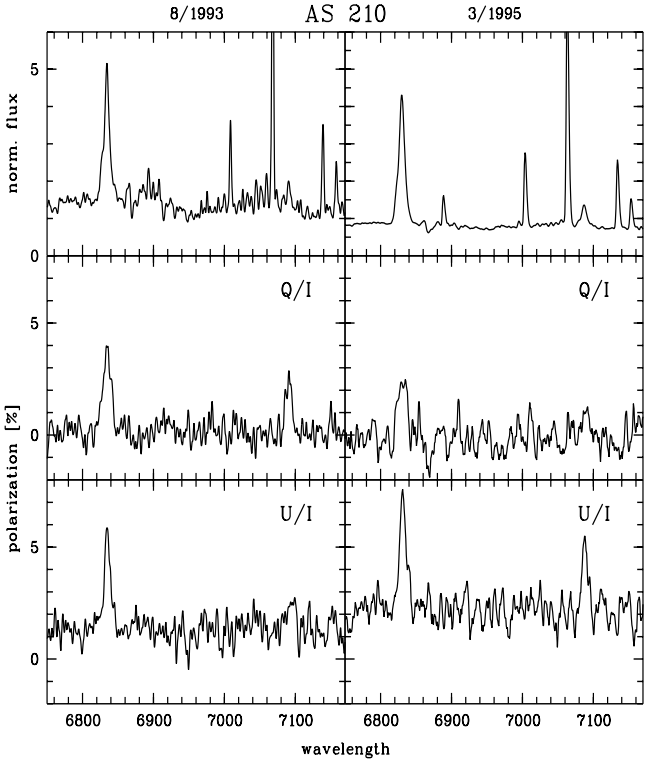

Fig. 1. Spectropolarimetry of AS 210 for August 1993 (left) and March 1995 (right). The top panels show the changes in the intensity spectrum due to the highly structured and variable spectrum of the carbon Mira, which is strong in 1993 and almost absent in 1995. In the normalized Stokes spectra Q/I and U/I the two Raman lines at λ6825 and λ7082 stand out clearly. The temporal rotation of the polarization angle in the Raman lines can be noticed as decrease in Q/I and simultaneous increase in U/I from 1993 to 1995. In normalized Stokes spectra the S/N is roughly $\sim\sqrt{I}$ and therefore low for the weak continuum. Despite the low S/N a change in the mean continuum polarization is visible (particularly in U/I) due to a variable intrinsic continuum component.

probably coupled to the strong intensity changes of the intrinsically polarized carbon-rich Mira variable. We therefore rely for an estimate of the interstellar polarization component on the polarization map of Harries & Howarth (1996b). Their Fig. 1(x) indicates that the continuum polarization of $1\%/53°$ as measured in May 1994 is compatible with the interstellar polarization measured for surrounding stars. However, the figure in Harries & Howarth (1996b) does not exclude the possibility that the interstellar polarization may be as large as 2% as measured in March 1995. We adopt here for AS 210 the value from Harries & Howarth (1996b) but note that it suffers from considerable uncertainty.

V1016 Cyg and RR Tel have a low continuum polarization. They display only small variations $\Delta p_c \approx 0.3\%$ in the percentage polarization but relatively large changes $\Delta\theta_c \gtrsim 20°$ in the position angle. Due to the low continuum polarization, already a small change in the intrinsic polarization can cause a substantial rotation in the position angle. We conclude that the interstellar correction is small and practically has no effect on the polarization of the Raman line (Sect. 4). For V1016 Cyg the variations in the continuum polarization are at the border

Table 3. Adopted interstellar polarization 6600–7200 Å. Unless noted otherwise, the uncertainties are of the order 0.1–0.2% in p_{is} and $\lesssim 3°$ in θ_{is}.

star	p_{is} [%]	θ_{is} [°]
Hen2-38	2.1	68
Hen2-106	2.9	66
Hen2-127	2.9	74
AS 210	1.0[a]	53
HM Sge	1.0	42
V1016 Cyg	0.3	109[b]
RR Tel	0.4	169[b]

[a] p_{is} could be as large as 2%.
[b] Estimated uncertainty of about $\Delta\theta_{is} = 5$–$15°$.

of significance. We therefore assume that the measured continuum polarization represents well the interstellar component. The polarization maps are of no help because the interstellar polarization in the sky region of V1016 Cyg is rather complicated. For simplicity we adopt here for the interstellar polarization of V1016 Cyg the value from our previous work (Schild & Schmid 1996).

For RR Tel the observed polarization changes including spectropolarimetric and photopolarimetric data are summarized in Brandi et al. (2000). The strongest variations are seen in the I-band where the variable red giant dominates the spectrum. In the U, B, V, R bands the polarization shows with the exception of a few measurements a rather constant value near $p \approx 0.5\%/\theta \approx 170°$. In these bands the emission is mainly nebular and therefore intrinsically unpolarized. The polarization map of surrounding stars (e.g. Schmid & Schild 1994) suggests a similar interstellar polarization component. We adopt for RR Tel $p_{is} = 0.4\%$, $\theta_{is} = 169°$ which is the mean of the three continuum polarization measurements from 1995 and 1999.

4. Polarization of the Raman lines

4.1. Integrated polarization

A simple polarimetric measure for an emission line is the integrated, flux weighted mean line polarization. Such a polarization parameter is independent of the spectral resolution and therefore well suited for a multi-epoch data set obtained with different instruments having possibly too low a resolution to resolve the Raman line profile.

The wavelength-integrated Stokes parameters I_ℓ, Q_ℓ and U_ℓ are measured from the intensity spectrum $I(\lambda)$ and the Stokes spectra $Q(\lambda)$ and $U(\lambda)$. In order to obtain the intrinsic polarization a correction for the interstellar contribution q_{is}, u_{is} must be applied according to

$$\frac{Q_L}{I_L} = \frac{Q_\ell}{I_\ell} - q_{is}$$

and similarly for the U_L/I_L component. From this, the intrinsic percentage polarization p_L and position angle θ_L can be calculated. The resulting integrated Raman line polarizations are given in Table 4, together with values from previous studies.

Table 4. Intrinsic line polarization for the λ6825 and λ7082 Raman lines. The polarization values are corrected for the interstellar contribution given in Table 3.

star	date	λ6825			λ7082			
		p_L [%]	θ_L [°]	errors [%/°]	p_L [%]	θ_L [°]	errors [%/°]	ref.
Hen2-38	6/92	2.43	21.5		2.80	32.3		SS94
	1/95	3.42	40.0	0.21/1.9	3.22	42.2	0.33/2.4	
	6/99	0.96	58.3	0.21/6.3	0.99	59.6	0.28/7.4	
Hen2-106	6/92	1.36	156.0		0.86	156.8		SS94
	1/95	<0.4			1.08	112.1	0.58/14.9	
	3/95	0.81	96.6	0.21/7.1	0.94	125.3	0.27/8.0	
	6/99	1.04	25.1	0.21/6.2	1.62	9.1	0.25/4.5	
Hen2-127	6/92	6.23	137.2		3.91	126.2		SS94
	3/95	3.45	145.2	0.26/2.4	2.70	153.1	0.62/6.5	
	6/99	5.90	168.0	0.23/1.5	5.11	168.2	0.39/2.4	
AS 210	5/93	7.08	26.3	1.08/1.5	>3.4	19.1	/4.3	
	8/93	8.29	22.5	0.63/1.3			too noisy	
	3/95	7.17	31.8	0.38/1.5	11.02	36.7	4.41/2.8	
	6/97	5.94	32.2	1.43/1.5	>1.8	32.5	/5.7	
	6/98	5.83	35.0	0.39/1.6	>2.6	27.7	/7.0	
	6/99	6.01	35.0	0.52/1.4	4.01	34.7	2.21/2.4	
HM Sge	6/98	3.4	34		3:	30:		S&00
	6/99	2.38	27.0	0.26/3.0	2.96	18.7	0.88/4.7	
V1016 Cyg	8/91	1.26	6.4		1.2	23.		SS96
	10/92	1.45	176.5		1.6:	177:		SS96
	5/93	1.88	172.9		1.6	3.8		SS96
	9/94	2.07	167.0		1.5	6.4		SS96
	6/97	2.98	168.4	0.22/1.2	1.27	179.6	0.27/3.8	
	6/98	2.83	161.8	0.21/2.3	1.52	171.0	0.25/4.1	
RR Tel	6/92	9.22	11.9		5.64	15.6		SS94
	3/95	8.39	14.6	0.21/1.2	5.74	13.6	0.29/1.6	
	6/99	9.09	21.4	0.20/1.2	6.87	18.7	0.43/1.4	
	8/99	9.04	21.0	0.30/1.2	7.64	18.8	1.30/1.5	

SS94: intrinsic line polarization reevaluated from the measured line polarization p_ℓ,θ_ℓ given in Schmid & Schild (1994) with the new interstellar polarization correction of Table 3;
S&00: Schmid et al. (2000); SS96: Schild & Schmid (1996).

The integrated Stokes parameters I_ℓ, Q_ℓ and U_ℓ are simple line flux measurements in the Stokes spectra which are in most cases easy and straightforward to obtain. Usually the Raman lines are strong and well defined against a flat continuum spectrum. The uncertainty on the final percentage polarization due to the continuum definition is normally quite small, below $\Delta p < 0.1\%$ for the λ6825 line and of the order $\Delta p = 0.1$–0.5% for the weaker λ7082 line. An exception is AS 210 where the spectral features of the carbon star can occasionally be so strong that the line flux (and polarization p) of λ6825 can only be determined with a relative accuracy of about $\Delta I/I \approx 0.1$ ($\rightarrow \Delta p/p \approx 0.1$), while the weaker Raman line λ7082 can hardly be measured (see Fig. 1 left panel).

The Stokes Q and U continua are flat, close to zero except in cases with intrinsic continuum polarization. The accuracy of the integrated Raman line Stokes Q or U parameters depends mainly on the signal to noise ratio. The data quality depends on the read out and background noise levels, and the number of weak radiation hits which are just above the noise level and therefore hard to identify as such. Errors in the integrated line polarization from these sources are typically $\Delta p \lesssim 0.1\%$ for the λ6825 line and about $\Delta p \approx 0.1$–0.5% for the weaker λ7082 line. The error estimates in Table 4 include in addition an error of $\Delta p = 0.2\%$ and $\Delta\theta = 1^\circ$ to account for systematic errors due to residual instrumental offsets. All error sources are combined as independent errors (square roots of the sum of errors squared). The error in the polarization angle follows according to $\Delta\theta = 0.5 \arctan(\Delta p/p)$.

All polarimetric data, including the earlier measurements, have to be corrected for the same interstellar contribution. We therefore have re-evaluated the June 1992 measurements of Hen2-38, Hen2-106, Hen2-127 and RR Tel from Schmid & Schild (1994). We applied the new interstellar polarization correction (Table 3) to their measured line polarization parameters p_ℓ, θ_ℓ (Table 2 of Schmid & Schild 1994). For RR Tel and Hen2-127 the new values for the intrinsic line polarization p_L, θ_L remain practically unchanged. For Hen2-106 and particularly for Hen2-38 the interstellar correction is different and

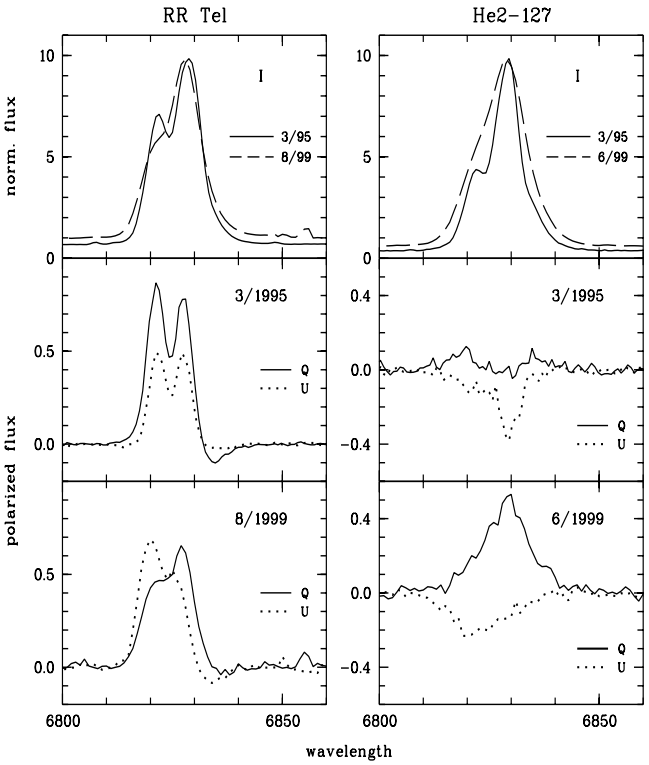

Fig. 2. Spectropolarimetry of the λ6825 Raman line in RR Tel and Hen2-127 for the years 1995 and 1999. The latter observations have a lower spectral resolution. The top panels show the intensity profiles and the middle and bottom panels the changes in the Stokes Q and U spectra between the two observations. The Stokes spectra are corrected for the interstellar polarization contribution according to Table 3.

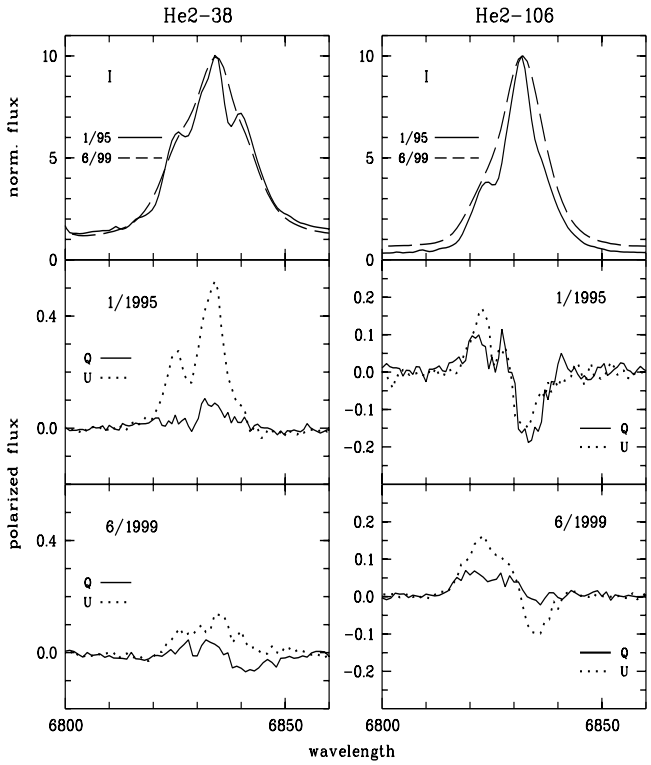

Fig. 3. Spectropolarimetry of the λ6825 Raman line in Hen2-38 and Hen2-106 for the years 1995 and 1999. See caption of Fig. 2 for details.

therefore the resulting intrinsic polarization also has changed. In the case of V1016 Cyg and HM Sge we have adopted the same interstellar polarization corrections as in the previous papers of Schild & Schmid (1996) and Schmid et al. (2000).

The uncertainties due to the interstellar polarization are not included in the error budget. As we are only interested in temporal polarization changes this is of secondary importance. A slightly different interstellar polarization would introduce in the normalized Stokes parameter plane $Q/I - U/I$ a small translation. However, the position angle on the sky and percentage polarization may depend critically on the applied interstellar correction in cases where the line polarization p_ℓ is small.

4.2. Line polarization structure

The Raman lines in symbiotic systems often show spectral structure across the polarization profile. It is mostly very subtle and only visible with high S/N and sufficient resolving power. In some systems the Raman line profile has components with opposite polarization of about equal strength. In these cases the integrated line polarization does not represent any of the polarization components, and it therefore carries little information. For these systems a different way of describing the polarization is necessary.

4.2.1. One dominant component

In our sample, only one dominant polarization component is seen in the systems AS 210 (Fig. 1), RR Tel and Hen2-127 (Fig. 2), Hen2-38 (Fig. 3, left), and HM Sge (see Schmid et al. 2000). In RR Tel the Stokes Q and U profiles show for March 1995 two strong polarization peaks in the center and blue wing of the Raman line. Because the ratio Q/U is practically the same for these two peaks also the polarization angle is constant. In the extreme red line wing ($\lambda > 6830$ Å) Stokes Q is negative indicating a different position angle, but this component is so weak that the position angle for the integrated line is practically unaffected. For the RR Tel observations of Aug. 1999 the blue and central peaks in the Q and U profiles have different strength. Thus the ratio Q/U and therefore the polarization angle rotates continuously from $\theta = 30°$ in the extreme blue wing, to 22.5° for $Q = U$ at 6825 Å, to 0° at 6830 Å where $U = 0$, and $\theta < 0°$ in the red line wing. The flux weighted polarization angle for the entire Raman line as measured for Aug. 1999 is 21° (Table 4). This value indicates $Q \cong U$ and seems to be representative of this line profile.

In the other systems of this group (Hen2-38, Hen2-127, AS 210 and HM Sge) the position angle rotation through the main polarization component is relatively small, i.e. comparable to the Aug. 1999 observations of RR Tel or smaller.

For all these objects the position angle from the integrated line polarization is representative of the entire Raman line. Using simply line integrated polarization parameters has the advantage that the measurement itself does not depend on the

Table 5. Line polarization structure for the λ6825 Raman line in Hen2-106 and V1016 Cyg. The polarization p_L in [%] and θ_L in [°] is given for 5 Å wide intervals from λ_1 = [6815–6820] to λ_6 = [6840–6845]. The values are corrected for the interstellar contribution given in Table 3. A colon indicates errors larger than about 2% and 10° in p_L and θ_L respectively. Only intervals with a line flux fraction $I_\lambda(\lambda_i)/I > 0.02$ are given.

date		λ_1	λ_2	λ_3	λ_4	λ_5	λ_6
Hen2-106							
Jan. 95	p_L	5.4:	4.7	0.6	2.4	2.4	1.2:
	θ_L	17:	29	12:	111	108	163:
	I_λ/I	.036	.125	.234	.352	.168	.055
March 95	p_L	3.1:	4.5	0.6	2.7	2.5	1.1:
	θ_L	16:	31	53:	106	113	117:
	I_λ/I	.032	.118	.220	.360	.181	.060
June 99	p_L	6.8:	4.6	1.7	0.4	1.3	1.9:
	θ_L	27:	34	32	146:	134	139:
	I_λ/I	.043	.119	.238	.325	.186	.062
V1016 Cyg							
Sep./Oct. 92	p_L	2.1	2.0	1.1	2.1	3.6:	
	θ_L	170	165	176	25	34:	
	I_λ/I	.127	.331	.337	.155	.031	
May 93	p_L	2.2	2.2	1.8	2.8	3.2:	
	θ_L	160	163	177	23	31	
	I_λ/I	.152	.331	.340	.136	.025	
Sep. 94	p_L	3.6	3.5	2.3	3.1	4.7:	
	θ_L	148	154	169	30	42:	
	I_λ/I	.123	.314	.338	.178	.032	
June 97	p_L	7.2	5.7	2.8	3.9	5.7:	
	θ_L	156	160	176	46	62:	
	I_λ/I	.145	.291	.346	.170	.034	
June 98	p_L	8.3	5.7	1.8	4.1	7.0:	
	θ_L	158	157	170	59	74:	
	I_λ/I	.165	.282	.341	.164	.032	

spectral resolution of the instrument, nor on the ambiguous definition of individual line components.

4.2.2. Multiple components

The situation is different for Hen2-106 and V1016 Cyg. In these systems, the overall polarization is low and there are two opposite polarization components with comparable strength, one in the blue and one in the red line portion (Fig. 3, right; and Schild & Schmid 1996). The normalized mean (integrated) line polarization is much less than the normalized polarization in the two components. In the case of Hen2-106 the blue and red line wings have a normalized polarization of about 2–5% or more, while the integrated line polarization is only about 1% or less. Thus, the two components with opposite polarization cancel each other so that the flux weighted mean polarization is not representative of either the blue or the red component (see Figs. 5 and 6).

For Hen2-106 and V1016 Cyg it is meaningful to measure the polarization for both components individually in order to account for the spectral structure. Table 5 gives the polarization parameters for 5 Å wide intervals through the λ6825 profile. For both stars we employ the interval λ_2 as representative for the polarization of the blue component. For the red component the interval λ_5 is taken for Hen2-106 and λ_4 for V1016 Cyg.

In order to have a longer time basis, we also include the line structure measurements from August 1991 of V1016 Cyg and June 1992 of Hen2-106 presented in Schmid & Schild (1994). We take from that work the polarization parameters for the wavelength intervals matching best the intervals λ_2 (blue) and λ_5 (red) defined here. For V1016 Cyg the corresponding parameters are p_L = 1.7%, θ_L = 178° for the blue and p_L = 1.6%, θ_L = 41° for the red interval. The interstellar polarization correction for V1016 Cyg is practically the same in both papers, so that we simply adopt the values from the previous work. For Hen2-106 we re-evaluate the polarization using the interstellar correction employed in this work. This yields for the June 1992 observation of Hen2-106 p_L = 2.9%, θ_L = 18° for the blue and p_L = 2.9%, θ_L = 146° for the red interval.

It is argued in the following section that the position angle of the blue polarization component best represents the system orientation.

5. Model expectations

For the interpretation of the changing Raman line polarization we adopt the basic scattering model for symbiotic systems (Schmid & Schild 1994; Schmid 1996; Harries & Howarth 1997; Lee & Lee 1997a,b). In this model the O VI $\lambda\lambda$1032, 1038 resonance lines are produced in an ionized region near the hot white dwarf and converted into Raman photons by neutral hydrogen in the extended atmosphere of the red giant. Because of the binary motion this asymmetric scattering geometry is rotating and produces phase locked variations in the scattering polarization. Such periodic variations have been detected in the Raman line polarizations of all short-period or S-type symbiotic systems that have been observed so far (Harries & Howarth 1996a, 2000; Schild & Schmid 1997; Schmid & Schild 1997a,b).

The models predict for a binary with a circular orbit and a fixed (corotating) scattering geometry that the orbital motion will in general produce oscillations in the percentage polarization and a rotation of the polarization angle. If the system is seen pole-on, the degree of polarization is high (right angle scattering situation) and constant but the polarization angle rotates at a constant rate. At a high orbital inclination the amplitude of the percentage polarization is large with maxima near high elongations and minima near conjunctions. The polarization angle changes slowly at high elongations and rapidly close to conjunctions. This is exactly what is observed in S-type systems where the polarization changes can be compared with radial velocity curves. For the wide D-type systems studied in this paper we have to expect elliptical orbits. This will produce additional changes of the rotation rate of the polarization angle and may also affect the scattering geometry due to changes in the stellar separation. Compared to circular orbits the observed variations in the line polarization are quantitatively modified (modulated) but qualitatively the behavior is not changed.

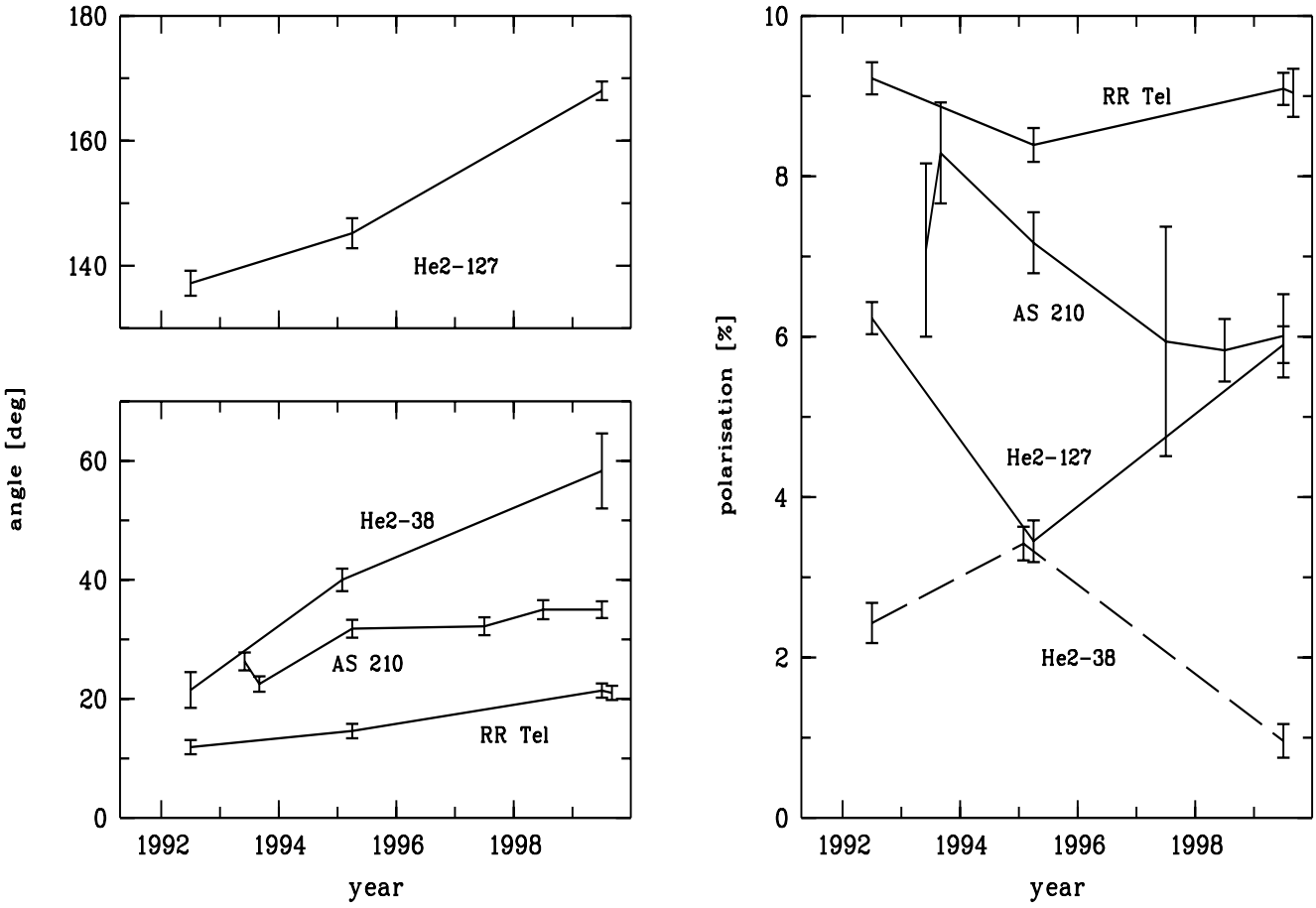

Fig. 4. Polarization changes in Hen2-38, Hen2-127, RR Tel and AS 210. These symbiotics display little or no polarization compensation and therefore the polarization angle (left panel) and percentage polarization (right) integrated over the full Raman line are shown.

5.1. Conjunction problem

Near conjunction the two stellar components are orientated along the line of sight and the O VI emission and scattering regions are alos expected to be aligned. In this forward or backward scattering situation only little polarization is expected because of the general rotational symmetry of the scattering situation. If the extended geometry is rotationally symmetric with respect to the line of sight, the polarization is zero because of geometric compensation. Only if the symmetry is broken does a net polarization result. Near conjunction this second order effect can be dominant. As a consequence the position angle is no longer a reliable indicator for the system orientation if the integrated line polarization is low, say near 1% or less. Such a low polarization is measured in all of the observations of Hen2-106, the last observation of Hen2-38 and the first few observations of V1016 Cyg. For these objects it is of importance to focus on the spectral structure in the polarization signal.

5.2. The polarization in the blue line wing

The spectral structure observed in the polarization signal of the Raman lines can be explained by the Doppler effect. Both the motion of the scattering particles in the red giants wind or/and the motion of the emitting O VI ions can be responsible for this. The favored model is that the observed profile is due to Doppler shifts introduced by the spherical motion of the scatterers in the wind of the red giant (e.g. Schmid & Schild 1994). According to this model the gas in the neutral region between the two stars is traveling towards the O VI region, so that the Raman scatterings produce blue shifted photons with a polarization perpendicular to the binary axis. This scattering region is strongly irradiated by O VI photons and geometrically well defined.

Surveys have shown that the blue component often strongly dominates the polarization of the Raman line. Therefore it can be expected that this component is a good indicator of the orientation of the stars in the binary system. In our sample this seems to be the case for Hen2-38, Hen2-127, AS 210, HM Sge, and RR Tel.

Hen2-106 and V1016 Cyg are systems with Raman lines having a blue and a red polarization component with comparable strength. Thereby the polarization angle differs strongly between the blue and red component as can be seen in Figs. 5 and 6. According to the above model the position angle in the blue component is still perpendicular to the binary axis, and therefore a good indicator of the system orientation. We suspect that the blue line polarization component is not dominant because we are seeing these systems close to conjunction.

The red component originates according to the models mentioned above from the outer wind regions of the Mira variable, where the gas is moving away from the O VI region and

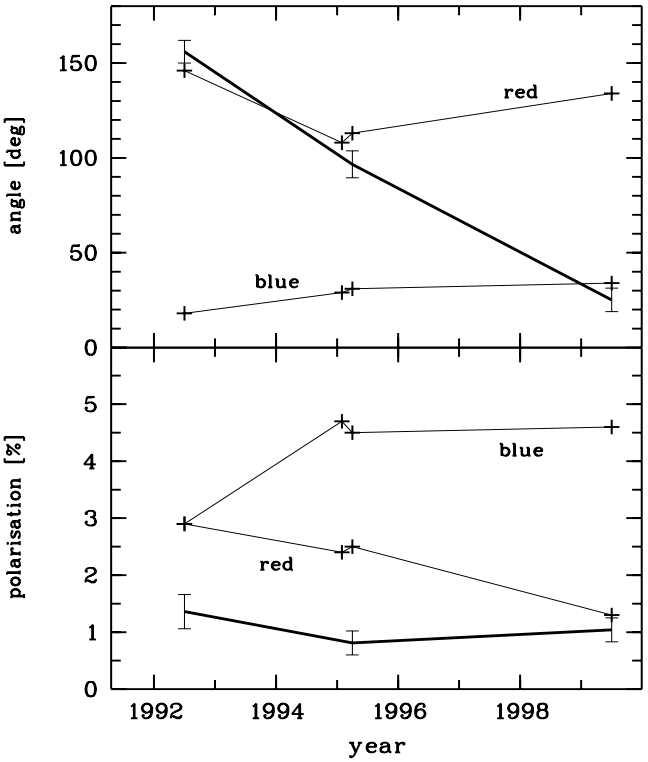

Fig. 5. Polarization changes in Hen2-106. The thick line shows the polarization parameters integrated over the full line and the thin lines the blue and red line components. The integrated parameters deviate strongly from the red and blue components which illustrates the effect of polarization compensation across the line profile.

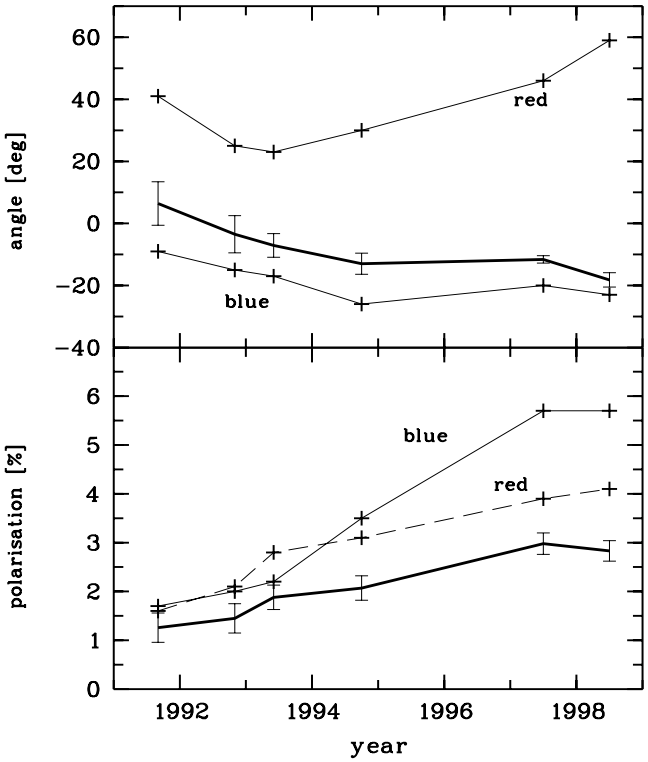

Fig. 6. The same as Fig. 5 but for V1016 Cyg.

the binary axis. Scatterings from this region produce red shifted Raman photons with an inclined or even parallel polarization relative to the binary axis. The geometry of this extended scattering region and the resulting scattering polarization is hard to predict and presumably is also variable due to the presence of radiative and hydrodynamical interaction processes between the two stellar components. Thus, the polarization component in the red line wing is in general not representative of the orientation of the system but rather of the distribution of the neutral gas further away from the Mira variable. For Hen2-106 and V1016 Cyg, which both have a low line polarization and a relatively strong red component, it therefore seems advisable to take the polarization in the blue line component as representative of the system orientation.

6. Orbital motion and configuration

6.1. Angle rotation and period

Guided by the models discussed in the previous chapter we base the interpretation of the angle rotation as an orbit indicator on the mean polarization parameters θ_L for the systems Hen2-38, Hen2-127, AS 210, HM Sge and RR Tel (Table 4) and the polarization angle in the interval λ_2 representing the blue line portion (Sect. 4.2, Table 5) for Hen2-106 and V1016 Cyg (Figs. 5 and 6).

In all our targets we see long-term polarization variations. For a few objects, the change in the polarization degree is marginal but the polarization angle always varies. For He 2-38, He 2-106 (blue) He 2-127, AS 210, and RR Tel the polarization angle is a steady, either decreasing or increasing function of time (Figs. 4 and 5). Such a steady behavior is indicative of changes in the scattering geometry due to orbital motion.

The observed angle changes can be fitted reasonably well with a linear function. Over a period of about ten years there are hardly any clear signs of changing rotation rates. V1016 Cyg may be an exception with an indication of a decelerating rotation in the blue line wing. The slopes $\Delta\theta_L/\Delta t$ resulting from a linear fit are given for the individual objects in Table 6. We find rotation rates in the range from 0.7 to 7°/yr. The slowest angle rotations are seen in RR Tel and Hen2-106. At present the fastest angle rotators are Hen2-38 and HM Sge but in the latter case the result is rather uncertain and remains to be confirmed. If these rates are taken to be representative for the full orbit, they yield an orbital period of the order of 400 yrs for RR Tel and Hen2-106 and 50 years for Hen2-38 and HM Sge. It is however to be expected that the orbits are inclined and elliptical, and since we still sample only a small fraction of an orbit, we expect future changes in the rotation rate. In a statistical way, however, the observations of all our targets taken together represent a mean orbit of a D-type symbiotic. We exclude HM Sge here because it has only two measurements separated by only one year. The average rotation rate of the other six objects is 2.5°/yr, which is equivalent to an orbital period of about 140 years. If we take the median rotation rate of 1.8°/yr the typical period increases to 200 years. Our observational coverage of 10 years is still short compared to these periods. If they are summed over all objects they however cover, in a statistical sense, a significant fraction of an average orbit.

Table 6. Variations in the λ6825 line polarization. The second column indicates whether the parameters refer to the total line polarization or only to the polarization in the blue portion of the line. $\Delta\theta_L/\Delta t$ is the mean rotation rate and $(p_{max} - p_{min})/p_{max}$ the relative variations in the percentage polarization. The last column gives the position angle of the binary axis projected onto the sky at epoch 1999.0.

star	θ_L	$\Delta\theta_L/\Delta t$ [°/yr]	$\frac{p_{max} - p_{min}}{p_{max}}$	PA [°] 1999.0
Hen2-38	total	5.1	0.72	147
Hen2-106	blue	0.7	0.04	124
Hen2-127	total	4.5	0.45	75
AS 210	total	1.8	0.30	127
HM Sge	total	-7 :[a]	0.30	120
V1016 Cyg	blue	-1.8	0.65	63
RR Tel	total	1.3	0.09	110

[a] High uncertainty due to the weak Raman line signal and the short time coverage.

As the orbits are likely inclined and possibly also elliptic we expect the rotation rates to change in the future. The rotation direction, i.e. the sign of the angle change should however remain fixed if our interpretation of orbital motion is correct. We note that the orbit of V1016 Cyg is retrograde, i.e. from North to West, whereas the others are prograde. For HM Sge, with only two measurements and weak Raman signals, we have to await further observations.

6.2. The orientation of the binary

Our polarimetry also yields information about the orientation of the binary system axes with respect to celestial coordinates. The standard scattering model requires that the orientation of the binary axis is perpendicular to the polarization angle in the blue portion of the Raman line. This is supported by the direct measurement of the orientation of the two stellar components in HM Sge by Eyres et al. (2001). They found practically the same orientation as previously derived from the Raman lines (Schmid et al. 2000).

Thus the measured position angles in the Raman line polarization provide a good measure for the system orientation. The mean rotation rate $\Delta\theta/\Delta t$ together with the position angle of the binary axis for the year $t_0 = 1999.0$ as derived by a linear regression fit to the polarization angle data is given in Table 6. The orientation of the binary is of interest for the interpretation of extended nebular structures. At present, circumstellar nebulosities are only observed for HM Sge (e.g. Eyres et al. 2001) and V1016 Cyg (e.g. Brocksopp et al. 2002) but future observations with improved spatial resolution will certainly reveal such nebula in other systems as well.

6.3. Orbit inclination

As outlined above the variability of the degree of polarization is linked to the orbital inclination. In particular we can select systems with low polarization as candidates seen near conjunction phase, because forward and backward scattering situation produce only little polarization. In our sample these are Hen2-38 and V1016 Cyg. The motion away or towards the conjunction phase is thereby expected to produce strong relative polarization changes. Such variations are listed in Table 6 as $(p_{max} - p_{min})/p_{max}$. Interestingly, this ratio suggests that Hen2-38 and V1016 Cyg have the highest relative polarization changes. This further supports that these systems are close to conjunction. For V1016 Cyg we see a systematic increase in the polarization, indicating that the system moves away from conjunction phase. The changes in Hen2-38 are less well covered, however, we may suspect that this system moves towards conjunction as the polarization disappeared practically for our most recent observation.

A high and relatively stable polarization as measured in particular for RR Tel, but also AS 210, suggests a right angle scattering situation that produces a high polarization. This requires that the binary axis lies close to the plane of the sky. Thus, these systems are candidates for being either low inclination systems or inclined systems seen near quadrature.

It should be kept in mind that the percentage polarization in the Raman lines does not only depend on the orientation of the binary axis but also on the scattering geometry. For example in Schmid (1996) it is shown with model calculations that the polarization is lowered by geometric compensation for systems with very extended scattering regions. We suspect that Hen2-106 could be a system with a red giant undergoing heavy mass loss giving rise to a very extended scattering region with significant geometric compensation. A high line polarization as observed for RR Tel is therefore probably a combination of both a right angle scattering situation and a compact hydrogen scattering region which could result in a system with a relatively low mass loss rate.

7. Discussion

This is a status report after the first decade of spectropolarimetric observations of the Raman features of selected symbiotic Miras. We clearly detect or confirm slow polarimetric changes, both in the angle and the degree of polarization. These changes can most easily be interpreted in terms of binary orbital motion. The present data is not sufficient to constrain the orbital period of any of the surveyed objects because the time coverage is still too short. Because of the unknown eccentricity and inclination it is at present not advisable to extrapolate from this short time coverage to a full orbit. In a statistical sense, however, we can determine a typical orbital period of about 150 yrs for D-type symbiotics. We demonstrate that polarimetry of the Raman lines can strongly support the long held suspicion that these symbiotics are long–period binaries. With the above period and a system mass of 2 $M_\odot$ a typical separation between the stellar components is 35 AU.

The apparent separation of the two stellar components follows from the distance. Distance determinations based on the period luminosity relation for Miras and measured pulsations periods are given in Whitelock (1987). She obtained distances for Hen2-38 ($d = 3.0$ kpc), Hen2-106 (2.8 kpc), V1016 Cyg (3.4 kpc), HM Sge (2.3 kpc), and RR Tel (2.5 kpc). With the

typical binary separation of 35 AU, this translates into apparent separations of the order 10–15 mas (milli-arcsec).

An instructive example that demonstrates both the power and caveats of polarimetric orbit deductions is V1016 Cyg. Six years ago Schild & Schmid (1996) deduced for this object an annual rotation rate of about 8°, a measurement based on four observations covering three years. More recent additional observations have shown that the angular rate of change has markedly decreased and in this paper we revise the annual rate down to about 2°. Although such discrepant results may be disturbing, they cannot invalidate the basic underlying scattering model. At least qualitatively, the polarimetric behaviour of V1016 Cyg can easily be understood: the early observations were close to conjunction, which means that the polarization was small and the angular rotation fast. Later the binary moves out of conjunction towards elongation and therefore the polarization degree increases rapidly but the angular rotation slows down. This is exactly what has been observed and at least at the present time there is no need to add further ingredients to the standard model. The lesson that has to be learnt is simply that one has to be patient and wait until a substantial fraction of the orbit has been covered observationally.

The link between orbital motion and polarization angle is closer than with the polarization degree (variability). At least part of the variability in p could be due to effects not related to the binary orbit. The impact of the Mira pulsations on the scattering polarization has not yet been studied. Strong changes are measured and expected in the Raman line due to temporal variations in the formation of dust in the outer wind regions (see Schmid et al. 2000). The available data are scarce and cover only a short time span, so that at present no firm statements can be made about the exact relation between the orbit inclination and the variations in p. However, with further data, the evolution in p could be informative for estimating the inclination of the systems.

The long-term effort required to establish accurate orbits raises a number of observational problems. It is desirable that all data are taken in a similar way in order to minimize systematic errors but polarimetric measurement equipment is likely to change over the years. Already now we had to combine data sets from different telescopes/spectrographs. A crucial point is also the spectral resolution. Occasionally, Stokes Q or U may have both positive and negative spectral parts across the Raman line. If unresolved, this spectral behavior will produce polarization results that are subject to spectral compensation and therefore difficult to interpret. It is important to measure the line polarization with a spectral resolution of about $\Delta\lambda \lesssim 2$ Å, so that the polarization in the blue portion of the Raman line can be measured separately. Up to now, all studies strongly support that the polarization in the blue wing of the λ6825 Raman line is the best indicator of the system orientation.

Acknowledgements. We are indebted to the WHT support astronomers who carried out the service observations. It is a pleasure to thank Jeremy Bailey (AAT), Chris Packham (WHT), and Ferdinando Patat (ESO), who provided valuable help during the observations.

References

Brandi, E., Garcia, L. G., Piirola, V., Scaltriti, F., & Quiroga, C. 2000, A&AS, 145, 197
Brocksopp, C., Bode, M. F., Eyres, S. P. S., et al. 2002, ApJ, 571, 947
Corradi, R. L. M., Ferrer, O. E., Schwarz, H. E., Brandi, E., & Garcia, L. 1999, A&A, 348, 978
Corradi, R. L. M., Livio, M., Balick, B., Munari, U., & Schwarz, H. E. 2001, ApJ, 553, 211
Espey, B. R., Schulte-Ladbeck, R. E., Kriss, G. A., et al. 1995, ApJ, 454, L61
Eyres, S. P. S., Bode, M. F., Taylor, A. R., Crocker, M. M., & Davis, R. J. 2001, ApJ, 551, 512
Harries, T. J., & Howarth, I. D. 1996a, A&A, 310, 235
Harries, T. J., & Howarth, I. D. 1996b, A&AS, 119, 61
Harries, T. J., & Howarth, I. D. 1997, A&AS, 121, 15
Harries, T. J., & Howarth, I. D. 2000, A&A, 361, 139
Hsu, J.-C., & Breger, M. 1982, ApJ, 262, 732
Lee, H.-W., & Lee, K. W. 1997a, MNRAS, 287, 211
Lee, K. W., & Lee, H.-W. 1997b, MNRAS, 292, 573
Schild, H., & Schmid, H. M. 1996, A&A, 310, 211
Schild, H., & Schmid, H. M. 1997, A&A, 324, 606
Schmid, H. M. 1989, A&A, 211, L31
Schmid, H. M. 1995, MNRAS, 275, 227
Schmid, H. M. 1996, MNRAS, 282, 511
Schmid, H. M., & Nussbaumer, H. 1993, A&A, 268, 159
Schmid, H. M., & Schild, H. 1994, A&A, 281, 145
Schmid, H. M., & Schild, H. 1997a, A&A, 321, 791
Schmid, H. M., & Schild, H. 1997b, A&A, 327, 219
Schmid, H. M., Krautter, J., Appenzeller, I., et al. 1999, A&A, 348, 950
Schmid, H. M., Corradi, R., Krautter, J., & Schild, H. 2000, A&A, 355, 261
Schmid, H. M., Appenzeller, I., Camenzind, M., et al. 2001, A&A, 372, 59
Serkowski, K., Mathewson, D. L., & Ford, V. L. 1975, ApJ, 196, 261
Whitelock, P. A. 1987, PASP, 99, 573